Effect of the Axial Ligand on Substrate Sulfoxidation Mediated by Iron(IV)–Oxo Porphyrin Cation Radical Oxidants

ARTICLE *in* CHEMISTRY - A EUROPEAN JOURNAL · APRIL 2011

Impact Factor: 5.73 · DOI: 10.1002/chem.201003187 · Source: PubMed

3 AUTHORS:

Devesh Kumar
Babasaheb Bhimrao Ambedkar University
100 PUBLICATIONS **4,052** CITATIONS
SEE PROFILE

G Narahari Sastry
Indian Institute of Chemical Technology
262 PUBLICATIONS **5,262** CITATIONS
SEE PROFILE

Sam de Visser
The University of Manchester
178 PUBLICATIONS **7,496** CITATIONS
SEE PROFILE

CHEMISTRY
A EUROPEAN JOURNAL

DOI: 10.1002/chem.201003187

Effect of the Axial Ligand on Substrate Sulfoxidation Mediated by Iron(IV)–Oxo Porphyrin Cation Radical Oxidants

Devesh Kumar,*[a] G. Narahari Sastry,[a] and Sam P. de Visser*[b]

Abstract: Cytochromes P450 catalyze a range of different oxygen-transfer processes including aliphatic and aromatic hydroxylation, epoxidation, and sulfoxidation reactions. Herein, we have investigated substrate sulfoxidation mediated by models of P450 enzymes as well as by biomimetic oxidants using density functional-theory methods and we have rationalized the sulfoxidation reaction barriers and rate constants. We carried out two sets of calculations: first, we calculated the sulfoxidation by an iron(IV)–oxo porphyrin cation radical oxidant [Fe^{IV}=O($Por^{+\bullet}$)SH] that mimics the active site of cytochrome P450 enzymes with a range of different substrates, and second, we studied one substrate (dimethyl sulfide) with a selection of different iron(IV)–oxo porphyrin cation radical oxidants [Fe^{IV}=O($Por^{+\bullet}$)L] with varying axial ligands L. The study presented herein shows that the barrier height for substrate sulfoxidation correlates linearly with the ionization potential of the substrate, thus reflecting the electron-transfer processes in the rate-determining step of the reaction. Furthermore, the axial ligand of the oxidant influences the pK_a value of the iron(IV)–oxo group, and, as a consequence, the bond dissociation energy (BDE_{OH}) value correlates with the barrier height for the reverse sulfoxidation reaction. These studies have generalized substrate-sulfoxidation reactions and have shown how they fundamentally compare with substrate hydroxylation and epoxidation reactions.

Keywords: axial ligands · cytochrome P450 · dioxygen activation · heme proteins · enzyme models

Introduction

Iron(IV)–oxo oxidants are powerful oxygen-transfer catalysts and have been identified as the active species of several enzymes including the cytochromes P450.[1] They are involved in important biochemical transformations ranging from biodegradation of toxic compounds in the liver to the biosynthesis of hormones in the body. Furthermore, they catalyze vital drug-metabolism reactions and, as such, the understanding of their mechanism and function is of great interest to the biotechnology field and the pharmaceutical industry.[1e] These enzymes are highly versatile and catalyze oxygen-transfer reactions (monoxygenation), ranging from aliphatic and aromatic hydroxylation to epoxidation and sulfoxidation.

Sulfoxidation reactions are catalyzed by many P450 isozymes.[2] For instance, the metabolism of the pesticide aldicarb and the biodegradation of neuroleptic drugs in the liver are associated with substrate sulfoxidation by P450 isozymes.[3] Detailed studies of the reaction mechanism of P450 enzymes and biomimetic complexes for substrate-sulfoxidation reactions have been reported[4] and give evidence of a concerted reaction mechanism. These studies are supported by density functional theory (DFT) and quantum mechanics/molecular mechanics (QM/MM) studies that highlight the iron(IV)–oxo heme cation radical (Compound I; Cpd I in Figure 1) as the active oxidant.[5] Furthermore, the experimental studies of Watanabe et al. implicated a relationship between the rate constant of substrate sulfoxidation by P450 enzymes and the ionization potential (IE) of the substrate.[6] Indeed, recent computational-modeling studies explained this correlation with electron-transfer mechanisms and a valence bond (VB) curve-crossing model.[7]

However, the first enzymatic iron(IV)–oxo heme cation radical species that has been characterized spectroscopically by using a combination of X-ray crystallographic studies,[8] was not that of cytochrome P450, but of the related enzyme horseradish peroxidase (HRP). The fundamental difference in the structure of the active site of HRP and P450 enzymes is the nature of the axial ligand (*trans* to the oxo group in Cpd I), which is a histidine ligand in HRP (His_{170} in Figure 2), but a cysteinate ligand in the P450s. Experimental studies identified a strong axial-ligand effect on the reactivity of heme enzymes,[9] in which a cysteinate ligand causes a push effect, whereas a histidine axial ligand withdraws elec-

[a] Dr. D. Kumar, Dr. G. N. Sastry
Molecular Modelling Group
Indian Institute of Chemical Technology
Hyderabad 500-607 (India)
Fax: (+91) 40-27193016
E-mail: dkclcre@yahoo.com

[b] Dr. S. P. de Visser
The Manchester Interdisciplinary Biocentre
and the School of Chemical Engineering and Analytical Science
The University of Manchester, 131 Princess Street
Manchester M1 7DN (UK)
Fax: (+44) 161-3065201
E-mail: sam.devisser@manchester.ac.uk

Supporting information for this article is available on the WWW under http://dx.doi.org/10.1002/chem.201003187.

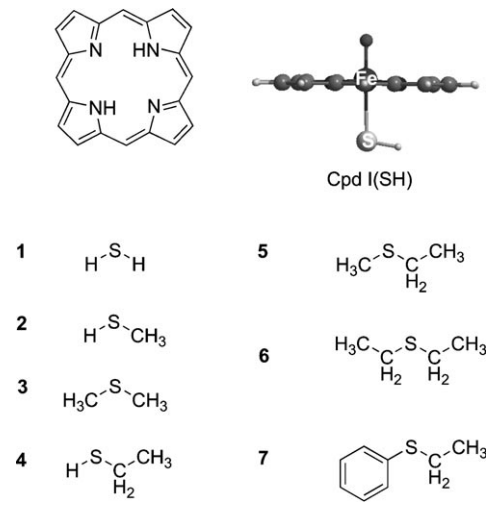

Figure 1. Oxidant and substrates used in this work.

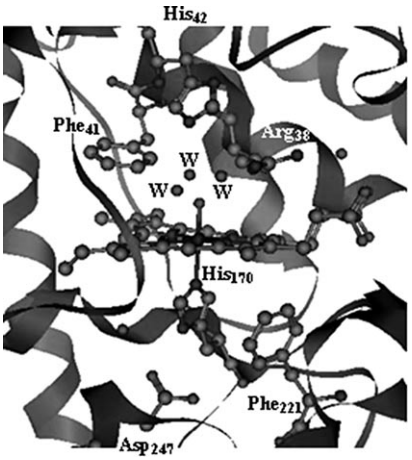

Figure 2. Structure of the active site of HRP (taken from the 1HCH pdb file). Amino acids labeled according to the pdb file, W = water molecules.

trons, thus resulting in a pull effect. As a consequence, this difference in push/pull effect of the axial ligand changes the central properties of the heme unit and results in functional differences. Further biomimetic studies by Gross and Nimri using iron(IV)–oxo tetramesitylporphyrin (TMP) cation radical oxidants with variable axial ligands showed a pronounced axial ligand effect on styrene epoxidation. These studies showed that electron-donating ligands lead to faster oxygen-transfer reactions, that is, higher rate constants, than systems with weaker electron-donating ligands.[10] More recent studies of Nam and co-workers[11] established a correlation between the reduction potential of the oxidant with the rate constant of hydrogen-atom abstraction. Additional computational studies[11b] showed that electron-donating axial ligands lower the triplet–quintet energy gap of the nonheme iron(IV)–oxo species, which thereby lowers the hydrogen-abstraction barriers of the substrates.

Figure 2 displays the structure of the active site of HRP as taken from the 1HCH protein databank (pdb) file.[12] The heme unit is linked to the protein through an interaction with a histidine axial ligand (His_{170}), which is involved in hydrogen-bonding interactions with a nearby carboxylic acid group of Asp_{247}. Also located on the axial site is an aromatic residue (Phe_{221}) that has been proposed to participate in electron-transfer processes from the reductase domain to the heme unit.[13] The amino acid residues Arg_{38} and His_{42} on the distal side are involved in proton-relay mechanisms in the catalytic cycle that generates Cpd I.

Electron nuclear double resonance (ENDOR) investigations on Cpd I of HRP revealed that the active species have an intriguing electronic configuration with three unpaired electrons: two in π^*_{FeO} orbitals located on the FeO group coupled to a heme-based cation radical in an orbital with a_{2u} symmetry.[14] This triplet pair of electrons on the Fe=O group is either ferromagnetically coupled to the heme radical into an overall quartet spin state or antiferromagnetically coupled into an overall doublet spin state. The nature of the electronic ground state, however, was shown to be sensitive to external conditions, whereby some experiments implicated a doublet-spin ground state, whereas others found a high-spin ground state.[15] Indeed, additional computational studies predicted the two spin states to be close in energy, that is, within about 1 kcal mol^{-1}.[16] Further computational studies showed that the degeneracy of the oxidant states also has consequences for substrate-activation mechanisms, which tend to lead to two-state reactivity (TSR) patterns with different rate constants and reaction mechanisms on both spin-state surfaces.[17] This TSR profile can result in the masquerade of kinetic isotope effects and the seemingly observance of multiple oxidants in the reaction mixture.

So far, most of the experimental and computational studies focused on the effect of the axial ligand on substrate hydroxylation and epoxidation by iron(IV)–oxo oxidants.[10,11,18,19] However, few studies have been reported on the effect of the axial ligand on substrate-sulfoxidation mechanisms by Cpd I species. Shaik and et al.[7] have recently reported substrate sulfoxidation by a Cpd I model of P450 using four *para*-substituted thioanisole compounds. The barrier heights of substrate sulfoxidation were found to be correlated to the IE of the substrate. Those studies, however, used only one oxidant and multiple substrates, whereas in this work we generalize the reactivity trends by investigating 1) one oxidant with multiple substrates and 2) one substrate with multiple oxidants. Thus, the primary focus of this paper is to investigate the fundamental properties that influence the barrier height of substrate-sulfoxidation reactions with a range of different oxidants.

Results and Discussion

We started our investigation with a detailed study of the reaction barriers of substrate sulfoxidation by Compound I of P450, which was modeled using a porphyrin unit without side chains and a thiolate axial ligand, [Fe^{IV}=O($Por^{+\bullet}$)SH] or designated Cpd I(SH). In contrast to the reported studies of Shaik et al.[7] we investigated a range of mainly aliphatic sul-

fides that differ in the length of the alkyl chain and range from a hydrogen atom to an ethyl group. Our selected range of substrates covers a much larger spread in ionization potentials, although not all substrates are natural sulfoxidation substrates by the P450s. Nevertheless, this series of substrates enables us to determine the rate constants and the barrier heights of a broad range of sulfoxidation reactions. Figure 1 shows the oxidant and the sulfide reactants that were used in this investigation, namely the reaction of Cpd I(SH) with hydrogen sulfide (**1**), methylmercaptane (**2**), dimethyl sulfide (**3**), ethylmercaptane (**4**), ethyl methyl sulfide (**5**), diethyl sulfide (**6**), and ethyl phenyl sulfide (**7**).

Cpd I(SH) has a degenerate doublet and quartet spin state as the ground state with the same orbital occupation: $(\pi^*_{xz})^1(\pi^*_{yz})^1(a_{2u})^1$. The former two orbitals are orthogonal π^*_{FeO} orbitals for the antibonding interactions of the metal $3d_{xz}/3d_{yz}$ atomic orbitals with $2p_x/2p_y$ orbitals on the oxo group. The a_{2u} orbital is a nonbonding orbital on the heme that is singly occupied, so that the reactant formally has an electronic configuration: $[Fe^{IV}{=}O(Por^{+\bullet})SH]$. We find the doublet and quartet spin states to be within 0.1 kcal mol^{-1}, which is in agreement with previous studies.[20] This degeneracy of the doublet and quartet spin state surfaces leads to two-state reactivity patterns with barriers and mechanisms on both spin state surfaces.[21] Often in aliphatic hydroxylation and epoxidation reactions the doublet and quartet barrier heights are close in energy,[22–24] but in the case of aromatic hydroxylation and sulfoxidation, significant differences in barrier heights, and consequently rate constants, were found between the two spin-state surfaces, thereby reducing the mechanism from two-state reactivity to single-state reactivity.[5,25]

Figure 3 shows an example of a typical potential energy surface for a sulfoxidation reaction, which was observed for the reaction of Cpd I(SH) with substrates **1–7**, in which we give the mechanism for ethyl methyl sulfide (**5**) sulfoxidation as an example. The reaction mechanisms obtained using the other substrates are similar although the energies are different. The inset of Figure 3 gives the barrier heights of substrate sulfoxidation with the other substrates. Thus, the reaction is concerted with a single barrier ($\mathbf{TS}_{SO}$) that separates the reactants from sulfoxide products (**P**). In the following, we will give the substrate in parenthesis behind these labels, for instance $^2\mathbf{TS}_{SO}(\mathbf{5})$ is the low-spin barrier for the sulfoxidation reaction of substrate **5** (ethyl methyl sulfide). The lowest lying barrier for sulfoxidation of substrate **5** is on the doublet spin state surface, which is 5.1 kcal mol^{-1} lower in energy than that found for the quartet spin state surface. This means that the reaction will proceed faster on the doublet spin state surface than on the quartet spin state surface. Consequently, the doublet spin state will dominate the reactivity, that is, a single-state reactivity on a doublet spin state surface will be expected. In a similar fashion, the other substrates (inset of Figure 3) also give $^2\mathbf{TS}_{SO}$ below $^4\mathbf{TS}_{SO}$ with an average doublet-quartet energy gap of (5.4 ± 1.2) kcal mol^{-1}. This spin-state ordering is in line with recent substrate-sulfoxidation studies by models of Cpd I of P450, which also gave a single-state reactivity mechanism on a dominant low spin state.[7]

The product complexes give the same spin-state ordering as the transition states with low spin below high spin. Previous studies on substrate hydroxylation and epoxidation mechanisms also gave doublet products below quartet-spin products.[23,24] The overall reaction is accomplished by a double-electron transfer from the substrate to the iron-porphyrin to give an iron(III)-porphyrin product complex with electronic configuration $(\pi^*_{xz})^2(\pi^*_{yz})^1(a_{2u})^2$ in $^2\mathbf{P}$ and $(\pi^*_{xz})^1(\pi^*_{yz})^1(\sigma^*_{z^2})^1(a_{2u})^2$ configuration in $^4\mathbf{P}$. Therefore, the double-electron transfer leads to the filling of the a_{2u} orbital with a second electron, whereas the other electron transfer occurs into the metal 3d system. Because the π^*_{xz} orbital is lower in energy than the $\sigma^*_{z^2}$ orbital, the doublet spin state is the lowest in energy for the product complexes. It was shown that the barrier height of substrate sulfoxidation correlates with the electron-transfer processes for the reaction,[7] hence substrate sulfoxidation should give a $^2\mathbf{TS}_{SO}$ below $^4\mathbf{TS}_{SO}$ barrier as indeed observed here. Interestingly, a recent quantum mechanics/molecular mechanics study on dimethyl sulfide sulfoxidation by Cpd I of two P450 isozymes ($P450_{cam}$ and $P450_{BM3}$) gave a quartet below doublet barrier,[5e] which im-

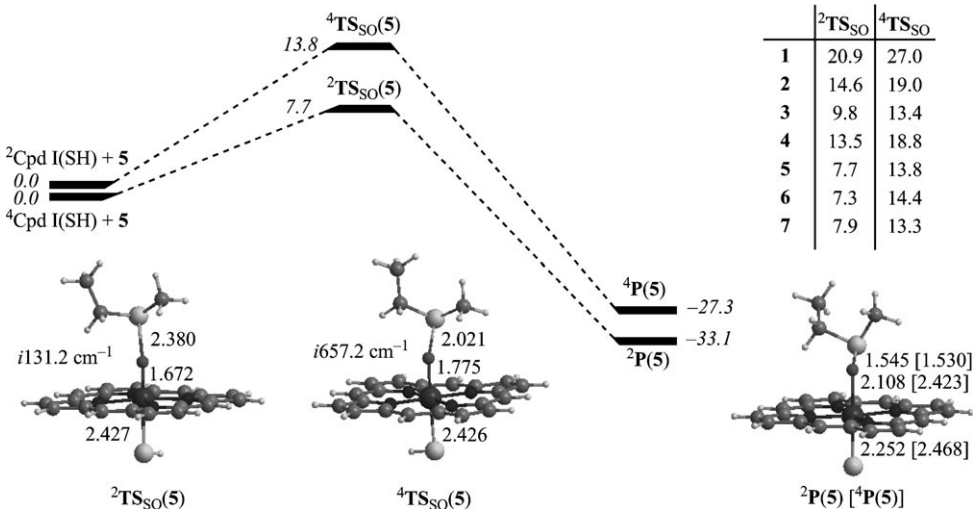

	^{2}TS$_{SO}$	^{4}TS$_{SO}$
1	20.9	27.0
2	14.6	19.0
3	9.8	13.4
4	13.5	18.8
5	7.7	13.8
6	7.3	14.4
7	7.9	13.3

Figure 3. Calculated potential-energy surface corresponding to the sulfoxidation of ethyl methyl sulfide (**5**) mediated by Cpd I(SH). All energies (kcal mol^{-1}) are relative to isolated reactants in the quartet spin state. Optimized geometries of $^{4,2}\mathbf{TS}_{SO}(\mathbf{5})$ and $^{4,2}\mathbf{P}(\mathbf{5})$ are also shown. Bond lengths are given in Ångstroms and the imaginary frequency in the transition state is in wave numbers. The table in the inset gives $^{4,2}\mathbf{TS}_{SO}$ barriers for the reaction of Cpd I(SH) with substrate **1–7** (kcal mol^{-1}).

plies that environmental perturbations, such as those in the substrate-binding pocket may influence the reactivity patterns and regioselectivity. This is particularly obvious from the differences in molecular geometry between ^{4}**TS**$_{SO}$ and ^{2}**TS**$_{SO}$ as can be seen in Figure 3. Thus, in most low-spin transition states in the gas phase the S–O bond is significantly longer than that found for the high-spin transition state, which may have consequences if the protein binding pocket was included in the model. In particular, inclusion of the protein binding pocket in the calculations as done in a QM/MM treatment may affect the relative energies of the low-spin and high-spin barriers because of their difference in interaction distance with nearby residues.

Optimized geometries of the doublet and quartet transition states of substrate **5** are shown in Figure 3, whereas the transition-state structures obtained using the other substrates are given in Figure 4. Figure 3 also displays the doublet and quartet product complexes, whereas the optimized geometries for the other complexes are summarized in the Supporting Information document. Generally, very little differences are observed among the various ^{2}**P** structures and similarly the ^{4}**P** structures are very much alike. Although we searched for correlations between bond distances and barrier height (Figure S12 in the Supporting Information), no obvious correlations were found. The best correlation coefficient ($R^2=0.78$) is found for the relationship between the low-spin barrier height and the O–S distance between oxidant and substrate. This trend implicates a low barrier for transition structures with long O–S distances and high barriers for transition structures with short O–S distances, which means that early transition states have the lowest barrier for the sulfoxidation reaction. The Fe–S distance in the transition states is very close for all structures with an average value of (2.432 ± 0.023) Å for ^{2}**TS**$_{SO}$ and (2.445 ± 0.015) Å for ^{4}**TS**$_{SO}$. The slightly longer distance obtained for the quartet spin state is due to electron transfer from the substrate into the $\sigma^*_{z^2}$ orbital that is antibonding along the Fe–S axis and therefore elongates the Fe–S bond. This effect is even more pronounced in the product complexes where the LS and HS Fe–S distances are separated by 0.216 Å. Furthermore, the Fe–O distances of the transition states are found in a narrow range with an average value of (1.700 ± 0.025) Å for ^{2}**TS**$_{SO}$ and (1.766 ± 0.033) Å for ^{4}**TS**$_{SO}$. Again, here the HS distance is slightly elongated with respect to the LS values owing to partial electron transfer from the substrate into the $\sigma^*_{z^2}$ orbital.

All transition states are characterized with a single imaginary frequency for the O–S stretch vibration. The ^{2}**TS**$_{SO}$ barriers have small imaginary frequencies ranging from *i*109.0 to *i*299.0 cm^{-1}, whereas the ^{4}**TS**$_{SO}$ barriers have much larger imaginary frequencies where values between *i*153.5–*i*771.9 cm^{-1} are found. These values imply that the shape of the potential-energy surface for substrate sulfoxidation on the doublet spin state surface is quite different from that found for the quartet spin state surface. Thus, the doublet spin state surface is broad and wide, whereas that for the quartet spin state surface is steeper and narrower around the barrier. In principle, this affects the amount of tunneling in the reaction.

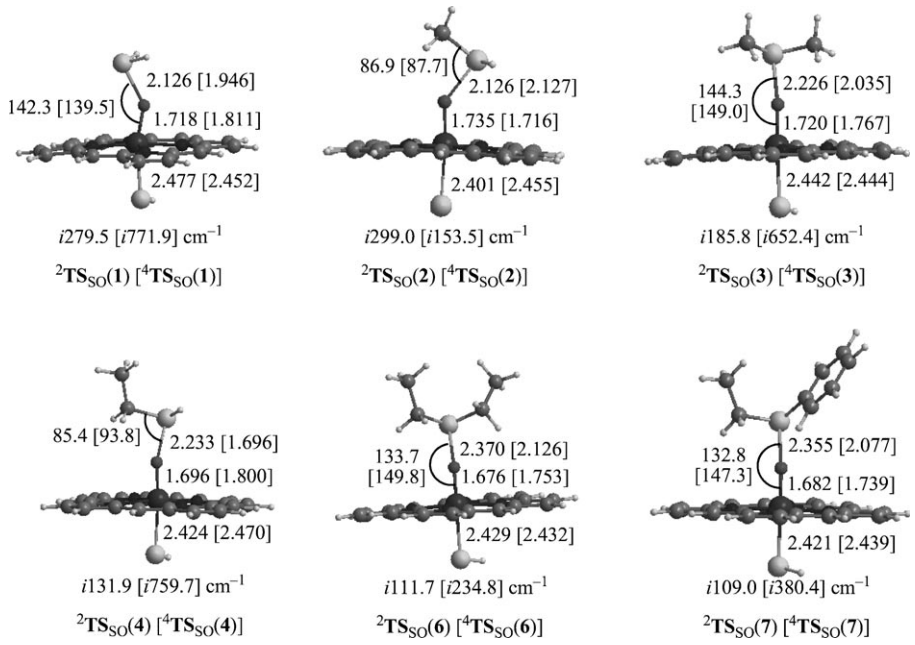

Figure 4. Optimized geometries of doublet and quartet transition states for the reaction of ^{4,2}Cpd I(SH) with substrates **1–4**, **6** and **7**. Bond lengths are in Ångstroms, angles in degrees and the imaginary frequency in the transition state is in wave numbers. For the structure of ^{4,2}**TS**$_{SO}$(**5**) see Figure 3.

Subsequently, we investigated the correlation between the height of the barrier for the sulfoxidation reaction (^{2}**TS**$_{SO}$) corresponding to the reaction of Cpd I(SH) with the series of substrates **1–7** and the IE of the substrate. The observed trends are displayed in Figure 5. The same trends were tested for the series of ^{4}**TS**$_{SO}$ barriers with ionization potential (Figure S11 in the Supporting Information), but the correlations are very similar, so we focused on the lowest lying barriers only, which proceed on the doublet spin potential energy surface. Calculated IE values of substrate correlate well with experimental data[26] with a systematic error of about 4 kcal mol^{-1}, as expected for DFT calculations at the B3LYP level of theory. As can be seen from Figure 5, the correlation coefficient is reasonable ($R^2=0.91$), which supports the hypothesis of a relationship between barrier height

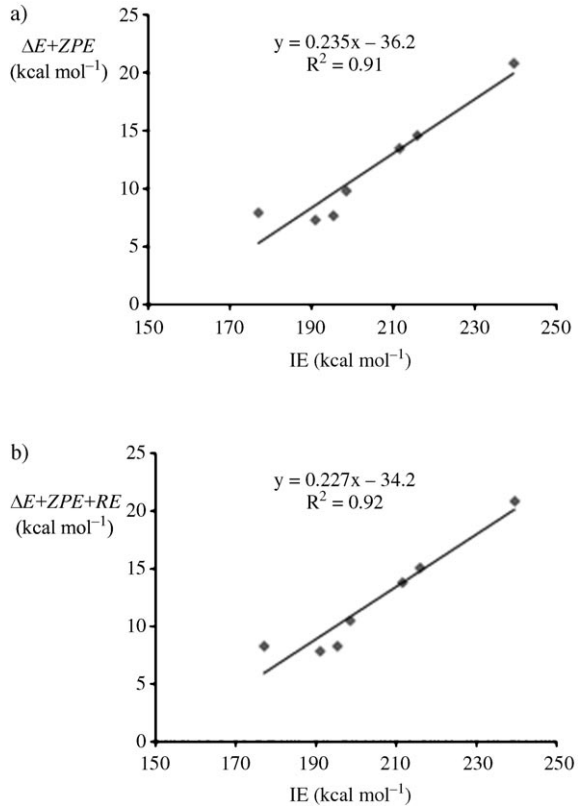

Figure 5. a) Correlation between the height of the barrier (^{2}**TS**$_{SO}$) for the reaction of ^{2}Cpd I(SH) with substrates **1**–**7** and the ionization energy of the substrate (IE). All values in kcal mol^{-1} and calculated with B3LYP. b) RE corrected barrier heights.

and IE. Following previous procedures,[23a] we also calculated the reorganization energy of the substrate (RE), which is defined as the energy of the substrate in the transition-state geometry minus that for the fully converged substrate structure. These RE values, however, are very small, that is, between 0.04 and 1.05 kcal mol^{-1} (Table S2 in the Supporting Information), so that an inclusion of its effect is minimal. The reason for these small values for RE come from the fact that substrate sulfoxidation is initiated by an attack of the oxo group of Cpd I on a lone pair of the sulfur atom of the substrate. This leads to very little geometric distortion in the transition-state geometry, hence the geometry of the substrate in the transition state is close to its fully relaxed structure, thus resulting in a small RE value. Inclusion of the RE value, (Figure 5b) therefore, gives only minor changes to the reactivity trends and the correlation coefficient between barrier height and IE changes slightly to $R^2 = 0.92$. Thus, our computational studies and reactivity trends are in perfect agreement with previous substrate sulfoxidation and epoxidation studies,[7,24] and implicate a linear correlation between barrier height and IE. Because rate constant and barrier heights are proportional to each other, also the rate constant of substrate sulfoxidation should connect with IE as indeed observed by Watanabe et al.[6] The correlation is consistent with the electron-transfer processes obtained from reactants to products that involve an electron transfer from substrate to oxidant. Moreover, the trend depicted in Figure 5 can be used to predict barrier heights of sulfide-sulfoxidation processes by [Fe^{IV}=O(Por$^{+\bullet}$)SH] using IE values of known substrates.

So far, we have reported the results obtained for one oxidant (Cpd I(SH)) with different sulfoxidation substrates. However, in a further set of calculations, we have searched for fundamental properties that correlate the barrier height of substrate sulfoxidation with a range of iron(IV)–oxo porphyrin cation radical oxidants Cpd I(L) with variable axial ligands L. Thermodynamically, in aliphatic hydroxylation reactions by iron(IV)–oxo oxidants, the reaction enthalpy and hence the driving force for the hydrogen atom abstraction by Cpd I(SH) or [Fe^{IV}=O(Por$^{+\bullet}$)SH] from substrates (SubH) is equal to the difference in strength of the C–H bond that is broken in the process and the O–H bond that is formed [Eqs. (1)–(3)].[27,28] However, apart from the driving force also the barrier height for the hydrogen-atom-abstraction reaction and consequently the rate constant is proportional to either BDE$_{CH}$ or BDE$_{OH}$.[23] These correlations have been rationalized by a VB curve crossing diagram that illustrated that the barrier heights of the reaction are connected to the electron-transfer processes involved in the reaction mechanism. In fact, these electron-transfer processes represent a singlet–triplet excitation in a C–H bond for aliphatic hydroxylation, which is proportional to BDE$_{CH}$, hence providing computational support for the observed trends. The computational studies revealed a correlation between barrier height of hydrogen-atom abstraction by Cpd I(SH) and BDE$_{CH}$,[23a] and a relationship between barrier height of hydrogen abstraction from propene by a range of iron(IV)–oxo oxidants proportional to the strength of the O–H bond formed in the process (BDE$_{OH}$).[23c]

$$[Fe^{IV}{=}O(Por^{+\bullet})SH]+SubH \rightarrow [Fe(OH)(Por)SH]+Sub^{\bullet} \quad (1)$$

$$\Delta H_{[Eq.\ (1)]} = BDE_{CH} - BDE_{OH} \quad (2)$$

$$AH \rightarrow A^{\bullet} + H^{\bullet} + BDE_{AH} \quad (3)$$

Recent studies of substrate-epoxidation reactions by metal–oxo oxidants found a correlation between the barrier height for the epoxidation reaction by Cpd I(SH) with the ionization energy of the substrate similar to what is shown here for substrate sulfoxidation.[25] This implies that the regioselectivity of substrate epoxidation versus sulfoxidation by Cpd I(SH) is determined by the IE of the substrate only. Accordingly, our studies implicate that the regioselectivity of epoxidation versus sulfoxidation in the enzyme can only be changed through favouring or disfavoring substrate binding processes in the substrate binding pocket.

Using a series of heme and nonheme Cpd I models with varying axial ligands, the substrate epoxidation reaction was studied computationally and was found to correlate with the BDE$_{OH}$ value of the oxidant.[24] Consequently, the formation of a C–O bond in a substrate epoxidation reaction was

found to be proportional to the formation of a H–O bond (BDE_{OH}). Therefore, to mimic the formation of an S–O bond in substrate-sulfoxidation reactions we investigated the correlation between the height of the barrier for substrate sulfoxidation and the BDE_{OH}. In particular, sulfoxidation reactions mediated by iron(IV)–oxo complexes follow the same electron-transfer mechanisms found in substrate epoxidation, in which the reaction of Cpd I(SH) with substrates correlates with IE(substrate). Therefore, we used one substrate (dimethyl sulfide, **3**) and investigated the sulfoxidation reaction using a series of iron(IV)–oxo porphyrin cation radical oxidants with variable axial ligands (L): Cpd I(L) with $L = SH^-$, OH^-, Cl^-, ImH, and CF_3COO^-. ImH is an imidazole-based ligand and as such Cpd I(ImH) represents a peroxidase Cpd I mimic. This set of oxidants span over a range of almost 20 kcal mol^{-1} in BDE_{OH} values, thus highlighting the effect of the axial ligand, where [Fe^{IV}=O($Por^{+\bullet}$)OH] is the system with the largest BDE_{OH} value (98.8 kcal mol^{-1}) and [Fe^{IV}=O($Por^{+\bullet}$)ImH] the one with the smallest BDE_{OH} value (79.4 kcal mol^{-1}). Although we again calculated the complete reaction mechanism similarly to that displayed in Figure 3, we now focus on the sulfoxidation transition states $^{4,2}\mathbf{TS}_{SO}$ only (for the complete set of data see the Supporting Information).

Figure 6 shows the optimized geometries of $^4\mathbf{TS}_{SO}(\mathbf{3}_L)$ with $L = OH^-$, Cl^-, ImH, and CF_3COO^-, whereas the $^4\mathbf{TS}_{SO}(\mathbf{3}_{SH})$ structure is given in Figure 4. Optimized geometries of $^4\mathbf{TS}_{SO}(\mathbf{3}_L)$ with $L = OH^-$, Cl^-, ImH, and CF_3COO^- are in good agreement with those observed and presented in Figure 3 and Figure 4 (see above). Also here the low-spin data follow the same trends and characteristics of the high-spin data, so that we will focus on the lowest lying barriers that pass $^4\mathbf{TS}_{SO}$ only. The Fe–O distance for $^4\mathbf{TS}_{SO}(\mathbf{3}_{OH})$ and $^4\mathbf{TS}_{SO}(\mathbf{3}_{Cl})$ is within the standard deviation of the values obtained in Figure 3 and Figure 4. The $^4\mathbf{TS}_{SO}$(ImH) structure, by contrast, has a very long Fe–O distance of 1.892 Å. Interestingly, the axial ligand has different effects on the transition state geometries than those discussed above regarding the mechanism of Cpd I(SH) with sulfides. No correlation between the length of the S–O bond and the barrier height is found for the axial-ligand studies presented in Figure 6. This implies that barrier height is determined by a set of intricate electron-transfer factors, which work in concordance or discordance as the substrate and oxidant varies, which precludes the correlation of barrier height with a single parameter.

Thus, the axial-ligand effect on substrate sulfoxidation manifests itself through differences in barrier height of the reaction processes that correlate with BDE_{OH}, Figure 6b. As follows from Figure 6b, the oxidant with the largest BDE_{OH} value reacts with dimethyl sulfide with the lowest reaction barriers, that is, highest rate constants, and therefore, will be the most effective oxidant of this series to perform substrate-sulfoxidation reactions. Although there is a bit of scatter in the data, the obtained correlation between barrier height and BDE_{OH} is reasonable ($R^2 = 0.90$) and is in good agreement with the trend of the axial-ligand effect found for

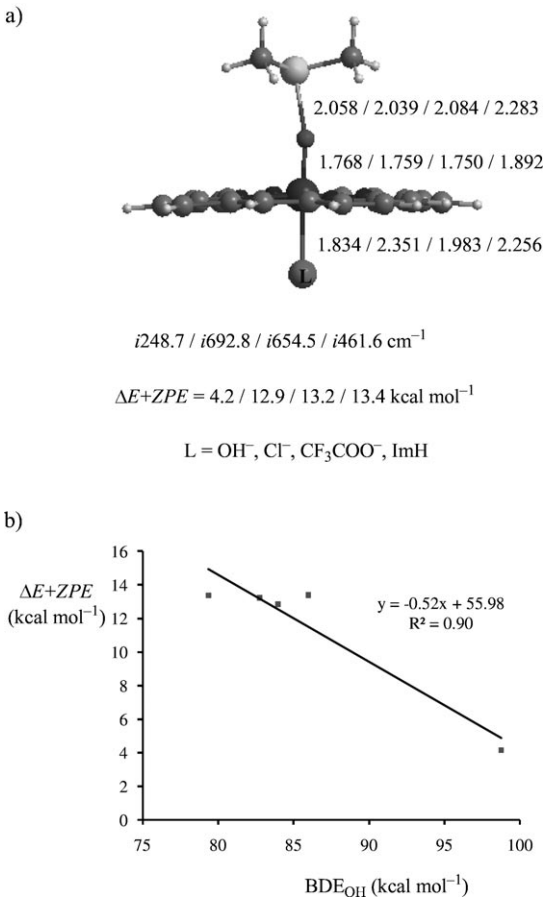

Figure 6. a) Optimized geometries of $^4\mathbf{TS}_{SO}(\mathbf{3}_L)$ with $L = OH^-$, Cl^-, ImH, and CF_3COO^-. Bond lengths are in Ångstroms and the imaginary frequencies are in wave numbers. b) Correlation between barrier height and BDE_{OH} value.

substrate epoxidation mediated by similar iron(IV)–oxo porphyrin cation radical oxidants.[24] Consequently, BDE_{OH} is a reasonably good representative of the axial-ligand effect in substrate sulfoxidation and the formation of a S–O bond can be faithfully mimicked with the formation of a H–O bond. Moreover, using known BDE_{OH} values for several oxidants, the catalytic potential in substrate sulfoxidation can be estimated (Figure 6b).

In addition to the correlations between the height of the barrier of a given reaction with the energetic properties (IE, BDE_{OH} etc), in the past we also established correlations between reaction enthalpy and reaction polarizability ($\Delta\alpha_r$).[28] Recent studies of reaction barriers of aliphatic hydroxylation and epoxidation mediated by iron(IV)–oxo complexes, reported a relationship between the barrier height and the change of polarizability volume between the reactant and the transition-state structures.[23c,24] To gain further insight into this unexpected relationship between polarizability difference and barrier height, we extracted the polarizability trace from the Gaussian frequency calculations and calculated the reaction polarizability ($\Delta\alpha_r$) using Equation (4). In this equation, the polarizability trace of the transition-state

structure, Cpd I and the substrate are given by α_{TS}, $\alpha_{Cpd\,I}$, and α_{SubH}, respectively.

$$\Delta\alpha_r = \alpha_{TS} - \alpha_{Cpd\,I} - \alpha_{SubH} \quad (4)$$

Figure 7 displays the correlation between reaction polarizability and barrier height for the high-spin and low-spin sulfoxidation reactions by Cpd I(SH). It appears that both trends give a reasonable linear correlation with a negative

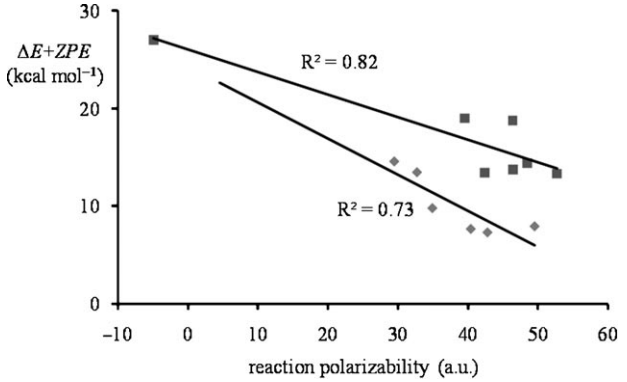

Figure 7. Correlation between the height of the barrier for substrate sulfoxidation and reaction polarizability for the high-spin (HS; ■) and low-spin (LS; ◆) mechanisms by Cpd I(SH).

slope, which implicates that high barriers are the result of larger changes in polarizability. Interestingly the reaction of ^{4}Cpd I(SH) with H_2S via ^{4}**TS**$_{SO}$(**1**) gives a negative reaction polarizability, which probably indicates that the reaction cannot take place on this spin-state surface. Note that polarizability does not correlate with the ionization potential,[29] so that the correlations shown in Figure 7 must have a different origin.

Experimental studies on substrate sulfoxidation by P450 enzymes gave a linear correlation between the log of the rate constant and the IE of the substrate.[6] Recent computational studies for the reaction of Cpd I(SH) with four *para*-substituted thioanisole substrates also gave a correlation between barrier height and substrate IE, which was rationalized by a VB curve-crossing diagram.[7,30] In this work, we found the same correlation between barrier height and substrate IE for the reaction of Cpd I(SH) with substrates. In addition, we show that the barrier height is proportional to the polarizability difference for the reaction and proportional to the barrier height for the reaction of dimethyl sulfide sulfoxidation mediated by metal–oxo oxidants and BDE_{OH}.

The observed trends are generalized in Figure 8 with a VB curve-crossing diagram for the sulfoxidation reaction.[7] The reaction starts from the left side with the wave function of the reactant (Ψ_r) and continues to the right to the wave function (Ψ_p) of the products. Thus, the reactant- and product-wave functions cross and lead to an avoided crossing and a transition state for substrate sulfoxidation ($\Delta E_{SO}^{\ddagger}$). The excited-state wave functions (Ψ_r* and Ψ_p*) are the re-

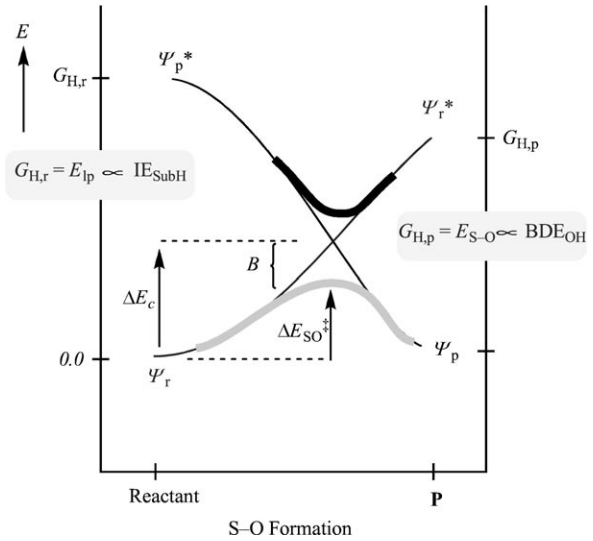

Figure 8. VB diagram for substrate sulfoxidation by Cpd I oxidants.

actant-wave function in the product geometry (Ψ_r*) and product-wave function in the reactant geometry (Ψ_p*). These wave functions are normally the electronic images of the states they correlate with, but here they represent the one-electron excitation energies.[30] Thus, the curve crossing between the reactant- and product-wave functions is located at a certain energy (ΔE_c), but the actual transition state ($\Delta E_{SO}^{\ddagger}$) for the sulfoxidation is lower in energy by a factor of *B*. It was further shown that the barrier height is proportional to a fraction (*f*) of the promotion gap in the reactant state ($G_{H,r}$) through

$$\Delta E_{SO}^{\ddagger} = f\,G_{H,r} - B \quad (5)$$

Thus, in the case of substrate sulfoxidation by iron(IV)–oxo complexes, the promotion gap $G_{H,r}$ represents the excitation energy of a lone pair of the substrate. Time dependent DFT calculations (TD-DFT) on the substrates showed that these excitation energies are proportional to the IE of the substrate, therefore, the VB diagram (Figure 8) predicts that IE should correlate with the height of the barrier for sulfoxidation as indeed shown in the described reactivity studies (Figure 5).

The reverse reaction from products to reactants has a barrier ($\Delta E_{SO,rev}^{\ddagger}$) that is proportional to $G_{H,p}$ rather than $G_{H,r}$ in Equation (5). The reverse sulfoxidation barrier is equal to the forward sulfoxidation barrier ($\Delta E_{SO}^{\ddagger}$) minus the reaction energy from reactants to products, that is, the driving force. Thus, $\Delta E_{SO,rev}^{\ddagger}$ involves two components: first, the one-electron oxidation of the heme group, in which the a_{2u} orbital is filled, and second, the energy for the S–O bond formation.[7] Hence, this step should correlate with the electron affinity of the oxidant, $EA_{Cpd\,I}$. The latter is connected to BDE_{OH} in combination with the pK_a value of Cpd I, [Eq. (6)].[31] The constant *C* constitutes factors including the ionization potential of a hydrogen atom as well as solvent corrections to the system.

$$BDE_{OH} = 23.06\,EA_{Cpd\,I} + 1.37\,pK_a + C \quad (6)$$

Therefore, the trends depicted in this work show that formation of an O–H bond is proportional to the formation of an O–S bond through BDE_{OH}. Interestingly, previous reactivity studies of substrate hydroxylation and epoxidation by a range of iron(IV)–oxo porphyrin cation radical complexes also showed a correlation with BDE_{OH}.[23c,24] This implies, therefore, that the regioselectivity of substrate hydroxylation, epoxidation, and sulfoxidation is not depending on the nature of the oxidant, because all these reactions correlate with BDE_{OH}. As a consequence, changing the axial ligand should not affect the regioselectivity of the process and of the observed product distributions. In all three cases the correlation of the height of the barrier with BDE_{OH} gives a slope in the region −0.52 to −0.76 and an intercept of 56.0 (sulfoxidation, Figure 6 b), 76.5 (hydroxylation, Ref. [23c]) and 79.7 (epoxidation, Ref. [24]). Thus, the hydroxylation and epoxidation curves are almost parallel with an equal slope and intercept that are within the error of the fitted curves. The intercept for substrate sulfoxidation is somewhat smaller, because a S–O bond is weaker than a O–H or C–O bond.

It is interesting to compare the reactions of oxygen-atom transfer from an iron(IV)–oxo porphyrin cation radical oxidant that result in the hydroxylation, epoxidation, and sulfoxidation of the substrate (Table 1). By varying the substrates and keeping the oxidant constant, we have shown that the intrinsic properties of the substrate determine the reaction barrier, and therefore the reaction kinetics. In the case of substrate epoxidation and sulfoxidation, the ionization potential of the substrate is the key for the reaction process, whereas in substrate hydroxylation the key is in the C–H bond strength of the substrate. In a similar way, we also investigated the effect of the oxidant on substrate hydroxylation, epoxidation, and sulfoxidation. In all processes, the rate-determining barrier involves the formation of a bond between the oxygen atom and one atom of the substrate (O–H bond in substrate hydroxylation, O–C bond for epoxidation, and O–S bond in sulfoxidation). These bond-formation steps can be successfully mimicked by the BDE_{OH} value of the oxidant. These studies, therefore, highlight the axial-ligand effect on substrate oxidation by metal–oxo oxidants.

Table 1. Properties of substrate and oxidant that affect the reaction barrier in the oxygen-transfer reaction mediated by iron(IV)–oxo porphyrin cation radicals.

	Intrinsic property that determines barrier height	
process	variable substrate	variable oxidant
sulfoxidation	IE	BDE_{OH}
epoxidation	IE	BDE_{OH}
hydroxylation	BDE_{CH}	BDE_{OH}

Conclusion

We have presented a systematic study carried out by means of density-functional theory on substrate sulfoxidation by iron(IV)–oxo porphyrin cation radical complexes and we have focused on the effect obtained by changing the axial ligand of the oxidant. To quantify the axial-ligand effect, we investigated the correlations between the heights of the barrier for the sulfoxidation reactions with the intrinsic properties of substrate and oxidant. Thus, the barrier heights of the sulfoxidation reaction correlate with the ionization potential of the substrate as well as with the BDE_{OH} of the oxidant. It is shown that the axial-ligand affects the BDE_{OH} value strongly and, in turn, this influences the rate constant of substrate sulfoxidation. We set up a VB curve-crossing diagram to explain the correlations. Furthermore, we showed that substrate sulfoxidation follows the same trends as substrate epoxidation, that is, is connected to the IE of the substrate and to the BDE_{OH} of the oxidant, which implies that the regioselectivity of epoxidation versus sulfoxidation should be constant with varying axial ligands.

Experimental Section

The procedures and methods used in this work are well-tested and benchmarked and have been applied to many reactivity studies of iron(IV)–oxo oxidants.[17,32] All geometries were fully optimized with the Jaguar 7.0 program package without geometric constraints and characterized as local minima or first order saddle points using an analytical frequency in Gaussian 03.[33,34] All transition states described in this work have a single imaginary frequency for the S–O stretch vibration, whereas local minima had real frequencies only. A double-ζ quality LACVP basis set on iron that includes a core potential combined with 6-31G** on the rest of the atoms (basis set B1) was used for geometry optimizations, frequencies, and initial geometry scans.[35] To test the effect of the basis set on the relative energies, we ran single point calculations using a triple-ζ quality LACV3P+ basis set on iron that contains a set of diffuse basis functions as well as a core potential in combination with 6–311+G* on the rest of the atoms (basis set B2). We use the B3LYP hybrid density functional method throughout,[36] as previous studies showed it to give good agreement with experimental rate constants.[37]

Following previous studies we simplified the iron(IV)–oxo species of P450 enzymes as protoporphyrin IX, whereby all side chains were replaced by hydrogen atoms.[20b] A thiolate axial ligand was used as it was shown to give a BDE_{OH} value close to a large active-site model with a CysGlyGly ligand system.[23e] To test the effect of the axial ligand on the reactivity patterns and trends, we replaced the axial ligand with Cl^-, OH^-, CF_3COO^-, and imidazole. All calculations were performed for the doublet and quartet spin state surfaces, which give similar trends. However, owing to space limitation we focused on the major trends only (see the supporting information for details).

Ionization potentials and BDE_{OH} values were calculated for isolated reactants at the same level of theory as described above. TD-DFT calculations were performed in Gaussian.[38]

Acknowledgements

The research was supported by CPU time provided by the National Service of Computational Chemistry Software (NSCCS). D.K. is Ramanujan Fellow of the Department of Science and Technology (New Delhi).

[1] a) M. Sono, M. P. Roach, E. D. Coulter, J. H. Dawson, *Chem. Rev.* **1996**, *96*, 2841–2888; b) F. P. Guengerich, *Chem. Res. Toxicol.* **2001**, *14*, 611–650; c) J. T. Groves, *Proc. Natl. Acad. Sci. USA* **2003**, *100*, 3569–3574; d) *Cytochrome P450: Structure, Mechanism and Biochemistry*, 3rd ed. (Ed.: P. R. Ortiz de Montellano), Kluwer Academic/Plenum Publishers, New York, **2004**; e) A. W. Munro, H. M. Girvan, K. J. McLean, *Nat. Prod. Rep.* **2007**, *24*, 585–609; f) *Handbook of Porphyrin Science* (Eds.. K. M. Kadish, K. M. Smith, R. Guilard), World Scientific, New Jersey, **2010**; g) P. R. Ortiz de Montellano, *Chem. Rev.* **2010**, *110*, 932–948.

[2] a) M. Werner, G. Birner, W, Dekant, *Chem. Res. Toxicol.* **1996**, *9*, 41–49; b) A. Madan, A. Parkinson, M. D. Faiman, *Drug Metab. Dispos.* **1995**, *23*, 1153–1158; c) K. A. Usmani, E. D. Karoly, E. Hodgson, R. L. Rose, *Drug Metab. Dispos.* **2004**, *32*, 333–339; d) B. Furnes, D. Schlenk, *Drug Metab. Dispos.* **2005**, *33*, 214–218.

[3] a) E. J. Perkins, A. El-Alfy, D. Schlenk, *Toxicol. Sci.* **1999**, *48*, 67–73; b) J. Wójcikowski, P. Maurel, W. A. Daniel, *Drug Metab. Disp.* **2006**, *34*, 471–476.

[4] a) Y. Goto, T. Matsui, S.-i. Ozaki, Y. Watanabe, S. Fukuzumi, *J. Am. Chem. Soc.* **1999**, *121*, 9497–9502; b) S. Kato, H.-J. Yang, T. Ueno, S.-i. Ozaki, G. N. Phillips, Jr., S. Fukuzumi, Y. Watanabe, *J. Am. Chem. Soc.* **2002**, *124*, 8506–8507; c) T. J. Volz, D. A. Rock, J. P. Jones, *J. Am. Chem. Soc.* **2002**, *124*, 9724–9725; d) K.-B. Cho, Y. Moreau, D. Kumar, D. A. Rock, J. P. Jones, S. Shaik, *Chem. Eur. J.* **2007**, *13*, 4103–4115; e) J. Benet-Buchholz, P. Comba, A. Llobet, S. Roeser, P. Vadivelu, S. Wiesner, *Dalton Trans.* **2010**, *39*, 3315–3320.

[5] a) P. K. Sharma, S. P. de Visser, S. Shaik, *J. Am. Chem. Soc.* **2003**, *125*, 8698–8699; b) D. Kumar, S. P. de Visser, P. K. Sharma, H. Hirao, S. Shaik, *Biochemistry* **2005**, *44*, 8148–8158; c) P. Rydberg, U. Ryde, L. Olsen, *J. Chem. Theory Comput.* **2008**, *4*, 1369–1377; d) C. Li, L. Zhang, C. Zhang, H. Hirao, W. Wu, S. Shaik, *Angew. Chem.* **2007**, *119*, 8316–8318; *Angew. Chem. Int. Ed.* **2007**, *46*, 8168–8170; e) C. S. Porro, M. J. Sutcliffe, S. P. de Visser, *J. Phys. Chem. A* **2009**, *113*, 11635–11642.

[6] a) Y. Watanabe, T. Iyanagi, S. Oae, *Tetrahedron Lett.* **1980**, *21*, 3685–3688; b) Y. Watanabe, T. Numata, T. Iyanagi, S. Oae, *Bull. Chem. Soc. Jpn.* **1981**, *54*, 1163–1170; c) Y. Watanabe, T. Iyanagi, S. Oae, *Tetrahedron Lett.* **1982**, *23*, 533–536.

[7] S. Shaik, Y. Wang, H. Chen, J. Song, R. Meir, *Faraday Discuss.* **2010**, *145*, 49–70.

[8] a) B. Chance, L. Powers, Y. Ching, T. L. Poulos, G. R. Schonbaum, I. Yamazaki, K. G. Paul, *Arch. Biochem. Biophys.* **1984**, *235*, 596–611; b) J. E. Penner-Hahn, K. Smith Eble, T. J. McMurry, M. Renner, A. L. Balch, J. T. Groves, J. H. Dawson, K. O. Hodgson, *J. Am. Chem. Soc.* **1986**, *108*, 7819–7825.

[9] J. H. Dawson, R. H. Holm, J. R. Trudell, G. Barth, R. E. Linder, E. Bunnenberg, C. Djerassi, S. C. Tang, *J. Am. Chem. Soc.* **1976**, *98*, 3707–3709.

[10] a) Z. Gross, S. Nimri, *Inorg. Chem.* **1994**, *33*, 1731–1732; b) Z. Gross, *J. Biol. Inorg. Chem.* **1996**, *1*, 368–371.

[11] a) C. V. Sastri, M. J. Park, T. Ohta, T. A. Jackson, A. Stubna, M. S. Seo, J. Lee, J. Kim, T. Kitagawa, E. Münck, L. Que Jr. , W. Nam, *J. Am. Chem. Soc.* **2005**, *127*, 12494–12495; b) C. V. Sastri, J. Lee, K. Oh, Y. J. Lee, J. Lee, T. A. Jackson, K. Ray, H. Hirao, W. Shin, J. A. Halfen, J. Kim, L. Que Jr. , S. Shaik, W. Nam, *Proc. Natl. Acad. Sci. USA* **2007**, *104*, 19181–19186; c) H. Hirao, L. Que Jr. , W. Nam, S. Shaik, *Chem. Eur. J.* **2008**, *14*, 1740–1756.

[12] G. I. Berglund, G. H. Carlsson, A. T. Smith, H. Szöke, A. Henriksen, J. Hajdu, *Nature* **2002**, *417*, 463–468.

[13] a) A. Morimoto, M. Tanaka, S. Takahashi, K. Ishimori, H. Hori, I. Morishima, *J. Biol. Chem.* **1998**, *273*, 14753–14760; b) B. D. Howes, N. C. Veitch, A. T. Smith, C. G. White, G. Smulevich, *Biochem. J.* **2001**, *353*, 181–191.

[14] a) J. E. Roberts, B. M. Hoffman, R. Rutter, L. P. Hager, *J. Am. Chem. Soc.* **1981**, *103*, 7654–7656; b) J. E. Roberts, B. M. Hoffman, R. Rutter, L. P. Hager, *J. Biol. Chem.* **1981**, *256*, 2118–2121.

[15] a) C. E. Schulz, R. Rutter, J. T. Sage, P. G. Debrunner, L. P. Hager, *Biochemistry* **1984**, *23*, 4743–4754; b) W.-J. Chuang, H. E. J. Van Wart, *J. Biol. Chem.* **1992**, *267*, 13293–13301; c) J. R. Kincaid, Y. Zheng, J. Al-Mustafa, K. Czarnecki, *J. Biol. Chem.* **1996**, *271*, 28805–28811.

[16] a) H. Kuramochi, L. Noodleman, D. A. Case, *J. Am. Chem. Soc.* **1997**, *119*, 11442–11451; b) R. J. Deeth, *J. Am. Chem. Soc.* **1999**, *121*, 6074–6075; c) M. T. Green, *J. Am. Chem. Soc.* **2000**, *122*, 9495–9499.

[17] a) S. Shaik, D. Kumar, S. P. de Visser, A. Altun, W. Thiel, *Chem. Rev.* **2005**, *105*, 2279–2328; b) S. Shaik, H. Hirao, D. Kumar, *Nat. Prod. Rep.* **2007**, *24*, 533–552.

[18] a) K. Czarnecki, S. Nimri, Z. Gross, L. M. Proniewicz, J. R. Kincaid, *J. Am. Chem. Soc.* **1996**, *118*, 2929–2935; b) T. Ohno, N. Suzuki, T. Dokoh, Y. Urano, K. Kikuchi, M. Hirobe, T. Higuchi, T. Nagano, *J. Inorg. Biochem.* **2000**, *82*, 123–125; c) W. J. Song, Y. O. Ryu, R. Song, W. Nam, *J. Biol. Inorg. Chem.* **2005**, *10*, 294–304; d) T. Yamane, K. Makino, N. Umezawa, N. Kato, T. Higuchi, *Angew. Chem.* **2008**, *120*, 6538–6540; *Angew. Chem. Int. Ed.* **2008**, *47*, 6438–6440; e) T. A. Jackson, J.-U. Rohde, M. S. Seo, C. V. Sastri, R. DeHont, A. Stubna, T. Ohta, T. Kitagawa, E. Münck, W. Nam, L. Que Jr, *J. Am. Chem. Soc.* **2008**, *130*, 12394–12407; f) A. Takahashi, T. Kurahashi, H. Fujii, *Inorg. Chem.* **2009**, *48*, 2614–2625; g) S. Fukuzumi, H. Kotani, T. Suenobu, S. Hong, Y.-M. Lee, W. Nam, *Chem. Eur. J.* **2009**, *15*, 354–361; h) M. E. Crestoni, S. Fornarini, F. Lanucara, *Chem. Eur. J.* **2009**, *15*, 7863–7866; i) Y. Kang, H. Chen, Y. J. Jeong, W. Lai, E. H. Bae, S. Shaik, W. Nam, *Chem. Eur. J.* **2009**, *15*, 10039–10046; j) K. A. Prokop, S. P. de Visser, D. P. Goldberg, *Angew. Chem.* **2010**, *122*, 5217–5221; *Angew. Chem. Int. Ed.* **2010**, *49*, 5091–5095; k) S. P. de Visser, R. Latifi, L. Tahsini, W. Nam, *Chem. Asian J.* **2011**, *6*, 493–504.

[19] a) T. Kamachi, T. Kouno, W. Nam, K. Yoshizawa, *J. Inorg. Biochem.* **2006**, *100*, 751–754; b) D. Kumar, S. P. de Visser, P. K. Sharma, E. Derat, S. Shaik, *J. Biol. Inorg. Chem.* **2005**, *10*, 181–189; c) S. P. de Visser, *J. Biol. Inorg. Chem.* **2006**, *11*, 168–178; d) S. P. de Visser, *J. Phys. Chem. B* **2006**, *110*, 20759–20761; e) S. P. de Visser, *J. Am. Chem. Soc.* **2006**, *128*, 15809–15818; f) S. P. de Visser, *J. Phys. Chem. B* **2007**, *111*, 12299–12302; g) S. P. de Visser, L. Tahsini, W. Nam, *Chem. Eur. J.* **2009**, *15*, 5577–5587.

[20] a) M. T. Green, *J. Am. Chem. Soc.* **1999**, *121*, 7939–7940; b) F. Ogliaro, S. P. de Visser, S. Cohen, J. Kaneti, S. Shaik, *ChemBioChem* **2001**, *2*, 848–851; c) S. P. de Visser, S. Shaik, P. K. Sharma, D. Kumar, W. Thiel, *J. Am. Chem. Soc.* **2003**, *125*, 15779–15788.

[21] S. Shaik, S. P. de Visser, F. Ogliaro, H. Schwarz, D. Schröder, *Curr. Opin. Chem. Biol.* **2002**, *6*, 556–567.

[22] a) T. Kamachi, K. Yoshizawa, *J. Am. Chem. Soc.* **2003**, *125*, 4652–4661; b) S. P. de Visser, D. Kumar, S. Cohen, R. Shacham, S. Shaik, *J. Am. Chem. Soc.* **2004**, *126*, 8362–8363.

[23] a) S. Shaik, D. Kumar, S. P. de Visser, *J. Am. Chem. Soc.* **2008**, *130*, 10128–10140; b) R. Latifi, M. Bagherzadeh, S. P. de Visser, *Chem. Eur. J.* **2009**, *15*, 6651–6662; c) S. P. de Visser, *J. Am. Chem. Soc.* **2010**, *132*, 1087–1097.

[24] D. Kumar, B. Karamzadeh, G. N. Sastry, S. P. de Visser, *J. Am. Chem. Soc.* **2010**, *132*, 7656–7667.

[25] S. P. de Visser, S. Shaik, *J. Am. Chem. Soc.* **2003**, *125*, 7413–7424.

[26] a) S. G. Lias, *Ionization Energy evaluation* in *NIST Chemistry Webbook* (Eds.: P. J. Linstrom, W. G. Mallard), National Institute of Standards and Technology, Gaithersburg, http://webbook.nist.gov, **2009**; b) K. Kimura, S. Katsumata, Y. Achiba, T. Yamazaki, S. Iwata, *Ionization Energies, ab initio Assignments, and Valence Electronic Structure for 200 Molecules in Handbook of HeI Photoelectron Spectra of Fundamental Organic Compounds*, Scientific Society Press, Tokyo, **1981**.

[27] a) J. M. Mayer, *Acc. Chem. Res.* **1998**, *31*, 441–450; b) J. M. Mayer, *Annu. Rev. Phys. Chem.* **2004**, *55*, 363–390; c) E. A. Mader, V. W. Manner, T. F. Markle, A. Wu, J. A. Franz, J. M. Mayer, *J. Am. Chem. Soc.* **2009**, *131*, 4335–4345; d) J. Kaizer, E. J. Klinker, N. Y. Oh, J.-U. Rohde, W. J. Song, A. Stubna, J. Kim, E. Münck, W. Nam, L. Que, Jr., *J. Am. Chem. Soc.* **2004**, *126*, 472–473; e) J. Yoon, S. A. Wilson, Y. K. Jang, M. S. Seo, K. Nehru, B. Hedman, K. O. Hodgson, E. Bill, E. I. Solomon, W. Nam, *Angew. Chem.* **2009**, *121*, 1283–

1286; *Angew. Chem. Int. Ed.* **2009**, *48*, 1257–1260; f) D. E. Lansky, D. P. Goldberg, *Inorg. Chem.* **2006**, *45*, 5119–5125; g) S. R. Bell, J. T. Groves, *J. Am. Chem. Soc.* **2009**, *131*, 9640–9641.
[28] S. P. de Visser, *Phys. Chem. Chem. Phys.* **1999**, *1*, 749–753.
[29] S. P. de Visser, unpublished results.
[30] S. Shaik, W. Lai, H. Chen, Y. Wang, *Acc. Chem. Res.* **2010**, *43*, 1154–1165.
[31] a) L. E. Friedrich, *J. Org. Chem.* **1983**, *48*, 3851–3852; b) F. G. Bordwell, J.-P. Cheng, *J. Am. Chem. Soc.* **1991**, *113*, 1736–1743; c) F. G. Bordwell, J.-P. Cheng, G.-Z. Ji, A. V. Satish, X. Zhang, *J. Am. Chem. Soc.* **1991**, *113*, 9790–9795.
[32] S. P. de Visser, W. Nam, *High-Valent Iron–Oxo Porphyrins in Oxygenation Reactions in Handbook of Porphyrin Science, Vol. 10* (Eds.: K. M. Kadish, K. M. Smith, R. Guilard), World Scientific Publishing, New Jersey, **2010**, Chapter 44, pp. 85–140.
[33] Jaguar 7.0, Schrödinger, LLC., New York **2007**.
[34] Gaussian 03, Revision C.01, M. J. Frisch, G. W. Trucks, H. B. Schlegel, G. E. Scuseria, M. A. Robb, J. R. Cheeseman, J. A. Montgomery, Jr., T. Vreven, K. N. Kudin, J. C. Burant, J. M. Millam, S. S. Iyengar, J. Tomasi, V. Barone, B. Mennucci, M. Cossi, G. Scalmani, N. Rega G. A. Petersson, H. Nakatsuji, M. Hada, M. Ehara, K. Toyota, R. Fukuda, J. Hasegawa, M. Ishida, T. Nakajima, Y. Honda, O. Kitao, N. Nakai, M. Klene, X. Li, J. E. Knox, H. P. Hratchian, J. B. Cross, C. Adamo, J. Jaramillo, R. Gomperts, R. E. Stratmann, O. Yazyev, A. J. Austin, R. Cammi, C. Pomelli, J. W. Ochterski, P. Y. Ayala, K. Morokuma, G. A., Voth, P. Salvador, J. J. Dannenberg, V. G. Zakrzewski, S. Dapprich, A. D. Daniels, M. C. Strain, O. Farkas, D. K. Malick, A. D. Rabuck, K. Raghavachari, J. B. Foresman, J. V. Ortiz, Q. Cui, A. G. Baboul, S. Clifford, J. Cioslowski, B. B. Stefanov, G. Liu, A. Liashenko, P. Piskorz, I. Komaromi, R. L. Martin, D. J. Fox, T. Keith, M. A. Al-Laham, C. Y. Peng, A., Nanayakkara, M. Challacombe, P. M. W. Gill, B. Johnson, W. Chen, M. W. Wong, C. Gonzalez, J. A. Pople, Gaussian, Inc., Wallingford CT, **2004**.
[35] a) P. J. Hay, W. R. Wadt, *J. Chem. Phys.* **1985**, *82*, 270–283; b) W. J. Hehre, R. Ditchfield, J. A. Pople, *J. Chem. Phys.* **1972**, *56*, 2257–2261.
[36] a) A. D. Becke, *J. Chem. Phys.* **1993**, *98*, 5648–5652; b) C. Lee, W. Yang, R. G. Parr, *Phys. Rev. B* **1988**, *37*, 785–789.
[37] S. P. de Visser, K. Oh, A.-R. Han, W. Nam, *Inorg. Chem.* **2007**, *46*, 4632–4641.
[38] R. Bauernschmitt, R. Ahlrichs, *Chem. Phys. Lett.* **1996**, *256*, 454–464.

Received: November 5, 2010
Published online: April 5, 2011

